SERI/TP-257-3490
UC Category: 261
DE90000312

Aerodynamic Testing of a Rotating Wind Turbine Blade

C. P. Butterfield
E. N. Nelsen

January 1990

Prepared for Solar '89
Denver, Colorado
19-22 June 1989

Prepared under Task No. WE911001

Solar Energy Research Institute
A Division of Midwest Research Institute

1617 Cole Boulevard
Golden, Colorado 80401-3393

Prepared for the
U.S. Department of Energy
Contract No. DE-AC02-83CH10093

NOTICE

This report was prepared as an account of work sponsored by an agency of the United States government. Neither the United States government nor any agency thereof, nor any of their employees, makes any warranty, express or implied, or assumes any legal liability or responsibility for the accuracy, completeness, or usefulness of any information, apparatus, product, or process disclosed, or represents that its use would not infringe privately owned rights. Reference herein to any specific commercial product, process, or service by trade name, trademark, manufacturer, or otherwise does not necessarily constitute or imply its endorsement, recommendation, or favoring by the United States government or any agency thereof. The views and opinions of authors expressed herein do not necessarily state or reflect those of the United States government or any agency thereof.

Printed in the United States of America
Available from:
National Technical Information Service
U.S. Department of Commerce
5285 Port Royal Road
Springfield, VA 22161

Price: Microfiche A01
Printed Copy A02

Codes are used for pricing all publications. The code is determined by the number of pages in the publication. Information pertaining to the pricing codes can be found in the current issue of the following publications which are generally available in most libraries: *Energy Research Abstracts (ERA)*; *Government Reports Announcements* and Index (*GRA* and I); *Scientific and Technical Abstract Reports (STAR)*; and publication NTIS-PR-360 available from NTIS at the above address.

AERODYNAMIC TESTING OF A ROTATING WIND TURBINE BLADE

C. P. Butterfield
E. N. Nelsen

Solar Energy Research Institute
1617 Cole Blvd.
Golden, CO 80401

ABSTRACT

Aerodynamic, load, flow-visualization, and inflow measurements were taken on a downwind horizontal-axis wind turbine (HAWT). A video camera mounted on the rotor recorded video images of tufts attached to the low-pressure side of the blade. Strain gages, mounted every 10% of the blade's span, provided load and pressure measurements. Pressure taps at 32 chordwise positions recorded pressure distributions. Wind inflow was measured via a vertical-plane array of anemometers located 10 m upwind.

The objectives of the test were to address whether airfoil pressure distributions measured on a rotating blade differed from those measured in the wind tunnel, if radial flow near or in the boundary layer of the airfoil affected pressure distributions, if dynamic stall could result in increased dynamic loads, and if the location of the separation boundary measured on the rotating blade agreed with that measured in two-dimensional flow in the wind tunnel.

1. INTRODUCTION

The analyses of HAWT aerodynamics assume that blade spanwise sections can be treated as independent airfoils operating in a two-dimensional, wind-tunnel-like flow condition. This assumption implies that there is no exchange of momentum in the spanwise direction. This has proven to be a reasonable assumption for HAWTs operating at medium to high tip-speed ratios. Even helicopters, which operate in a highly three-dimensional flow state, can be analyzed using two-dimensional airfoil data.

However, when stall occurs on a rotating HAWT blade, analytical predictions break down. In high winds, HAWTs actually produce more power and experience higher loads than standard analyses would predict using two-dimensional wind tunnel data. This unexplained increase in performance appears to be a steady-state phenomenon that researchers have called "delayed stall." Dynamic blade loads measured on HAWTs have been larger than predicted using existing aeroelastic analysis. This problem may be caused by inaccurately modeling complex inflow to the rotor. These analyses are typically capable of modeling simple wind shear and in some codes even complex steady-state wind shear. But even the complex model may not be accurate enough because it assumes a steady shear when actually the inflow is turbulent (i.e., constantly changing).

This may or may not be the explanation for the poor prediction of dynamic loads. Certainly, it is a contributor, but there may be other contributors, such as dynamic stall or spanwise flow. Both dynamic stall and spanwise flow have contributed to increasing loads on helicopter rotors. Engineers in the helicopter industry had to make detailed pressure measurements on blades and flow-visualization measurements before they were able to understand the complex fluid dynamic processes that caused these loads. The same is true for HAWTs. The results of this program will help determine (1) if aerodynamic forces are obeying two-dimensional airfoil characteristics, (2) how turbulent inflow must be transformed into a rotational frame of reference, and (3) if lift coefficients are reaching levels higher than those possible in two-dimensional flow. Pressure and flow-visualization measurements are the essential first step that must be taken before dynamic stall, spanwise flow, delayed stall, or other three-dimensional flow phenomena can be isolated. Once the dominant physical process is isolated, subsequent detailed test programs can focus on understanding and modifying it.

The test program described in this report was funded by the Department of Energy (DOE) and conducted by the Solar Energy Research Institute (SERI) at its Wind Energy Test Center (WETC) in Golden, Colorado. This test, called the "Combined Experiment," includes all the essential physical measurements just mentioned. We recorded flow patterns using a high-speed video camera mounted on the rotor to view small tufts mounted on the blade. We used pressure transducers and angle-of-attack

(AOA) probes to measure lift coefficients and corresponding angles of attack. Finally, we simultaneously made detailed, near-field inflow and blade-load measurements. These data will provide us with a comprehensive picture of the inflow profile, how that inflow affects aerodynamic loads, and how these aerodynamic loads correlate with structural loads. Although we present some typical preliminary results here, the test is still in progress and is expected to continue through the spring of 1990. Therefore, this report is merely an overview of the test program and not a comprehensive analysis of any results to date. Future reports will deal comprehensively with various topics.

2. TEST SETUP

The Grumman Wind Stream 33 was our test turbine. Figures 1 and 2 show the turbine's original characteristics. The Grumman turbine was an excellent test turbine for the Combined Experiment for the following reasons:

1. The rigid, three-bladed hub reduced the possibility of blade motion affecting the data.
2. A constant-chord, zero-twist, zero-thickness taper blade was incorporated to reduce the effects of blade geometry on stalled flow (because stalled characteristics can be affected by twist and thickness taper).
3. The Wind Stream 33's downwind configuration allowed us to mount a camera on a boom extending downwind and aimed at the low-pressure side of the blade, to allow us to easily view tufts mounted on the blade.
4. The machine and tower lent themselves to the modifications needed for the test, such as tilting the tower, mounting the transducer, and modifying the control system.
5. The pitch control system allowed variations in stall or AOA for any wind speed.

We modified the blade significantly. Although we maintained the original blade planform (constant-chord, zero-twist, zero-taper), we selected a new airfoil. There were no wind tunnel data for the production airfoil, and wind tunnel data are crucial for comparisons between two-dimensional and three-dimensional pressure distributions.

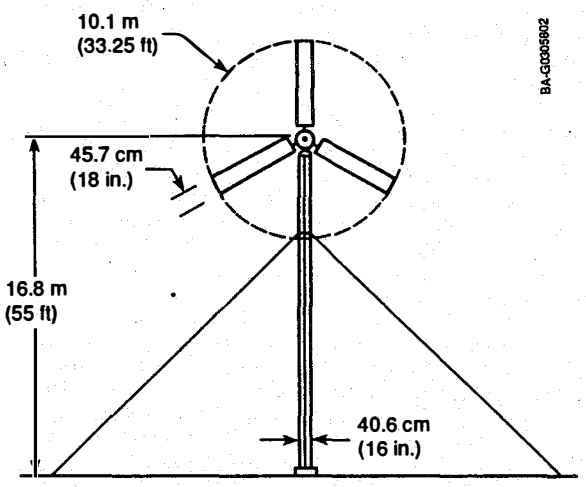

Windstream 33 Characteristics

Induction generator rating	20 kW
Induction generator speed range	1800-1860 rpm
Gearbox ratio	25.1:1
Rotor speed	74.1 rpm
Rotor diameter	33.25 ft
Rotor solidity	0.0615
Blade chord	1.5 ft
Power coefficient, Max ($C_{P\ MAX}$)	0.38°
Tip speed ratio at $C_{P\ MAX}$	5.25°
Wind speed at $C_{P\ MAX}$	17.0 mph
System efficiency at $C_{P\ MAX}$	83%
Output power at VW = 24 mph	15 kW*
Rotor coning angle	3-1/2°
Razor/Nacelle assembly wt.	2,589 lb.
Drive axis height	55 ft
Tower section	16.0 in./0 dia, 3/8 in. wall
Guy base	80 ft

*Predicted

Fig. 1. Characteristics of the Grumman WS33 wind turbine

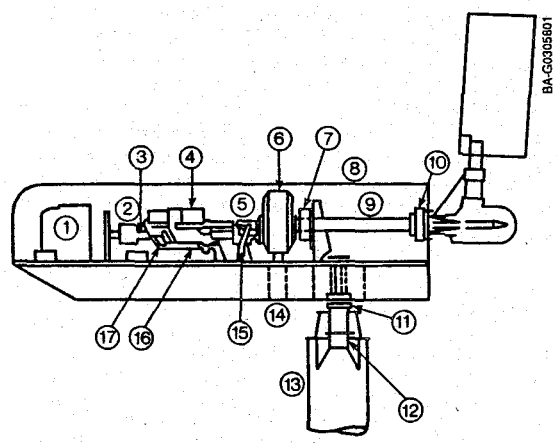

Fig. 2. Schematic diagram of the Grumman WS33 wind turbine

We chose an S809 airfoil developed by Airfoils, Inc. under contract to SERI (1). This airfoil is well documented, including two-dimensional pressure distributions, separation boundary locations, drag data, and flow-visualization data. The blade material is fiberglass composite, and the blades are designed to be as stiff as possible to limit blade deflections. The dynamics of the blade are tailored to avoid coalescence of rotor harmonics with flapwise, edgewise, and torsional natural frequencies. To minimize the possibility of aeroelastic instabilities, the mass and elastic axes are aligned with the aerodynamic axis. The instrumented blade was painted black to contrast the white tufts.

We used a guyed-pole tower with a hinged base and gin pole to be tilted down easily. An electric winch helped us to lower and raise the system to aid in instrumentation checks and calibration. We also paid careful attention to tower and foundation loads when designing this system.

The camera boom designed to hold the 10-lb, high-shutter-speed video camera was hinged at the base so that we could completely tilt down the tower. The boom had a system fundamental frequency of ten cycles per revolution (10P). The boom was mounted on the hub and extended downwind 10 ft on the axis of rotation. This boom length allowed a view angle of 30° at the tip of the blade and 45° at the 66% span. We mounted additional equipment on the boom, such as the data-acquisition system, the pressure system controller (PSC), and lighting for night testing (Figure 3).

We designed a remote-controlled yaw lock to allow us to set and release various yaw positions. This yaw retention system had a strain-gaged link to measure yaw moments.

We erected two Rohn 45G guyed meteorological (met) towers to the west-northwest (290° direction) of the test machine (Figure 4). At the WETC, winds historically come from this direction in the spring. The two towers supported three cross booms, where we mounted 13 anemometers in a vertical-plane array to measure the inflow. The R. M. Young U-V-W anemometers measure three components of wind speed and have a bandwidth of DC to approximately 1 Hz. We positioned them one rotor diameter (1D) upwind of the turbine. We placed two TSI X-type hot-wire anemometers near hub height on a third tower, just to the north of the vertical-plane array. The X-films provide measurements of horizontal and vertical wind velocity components at relatively high frequencies. Figure 4 shows the placement of these anemometers in a vertical-plane array, and also of the two TSI X-wire anemometers and one triaxial sonic anemometer on the separate "local met tower."

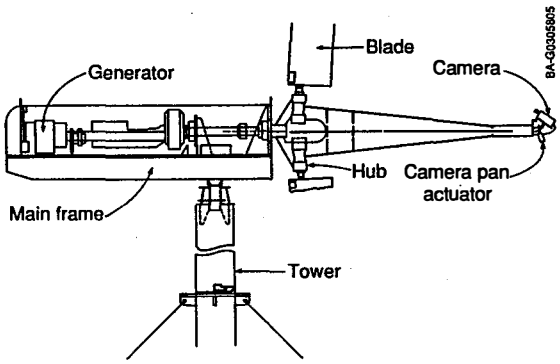

Fig. 3. Camera boom layout on the wind turbine

3. INSTRUMENTATION

3.1 Tufts

The tufts were of 100% polyester white thread measuring approximately 0.25 mm in diameter and 45 mm in length ("mini tufts"). We attached them to the downwind side of the blade with super glue. We spaced the rows of tufts 76 mm apart in the blade spanwise direction. The rows consisted of ten tufts placed in the chordwise direction, resulting in approximately one tuft for every 10% of the chord in the chordwise direction, and one tuft for every 1.5% of the span in the spanwise direction. The diameter of the tufts was chosen to minimize the effects on the boundary layer without making the tufts invisible to the video camera. Tufts that are large relative to the boundary layer thickness will cause transition and premature separation, which leads to a lower maximum lift coefficient ($C_{l,max}$). This effect is documented in (2).

3.2 Video Equipment

We installed a NISUS N-2000 video camera on a boom, and we put a recorder and monitor in

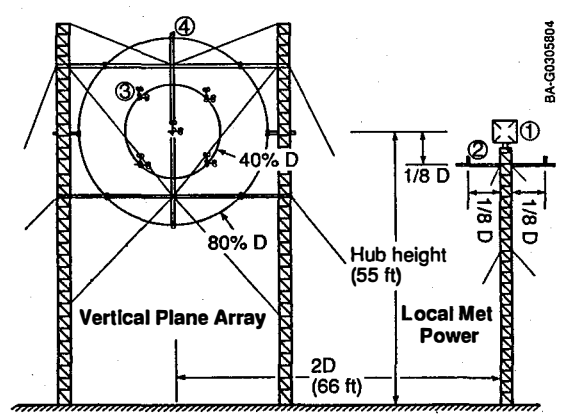

Item no.	Description
1	U-V-W sonic anemometer
2	Ruggedized TSI hot films
3	U-V-W gill anemometers
4	Prop vane anemometers

Fig. 4. Layout of the anemometers

the control house so that the test engineer could observe the blade-mounted tufts and adjust the test according to the desired flow condition. The camera used a mechanical shutter to freeze video frames in 1/625 of a second. Thirty video frames were recorded every second to allow one frame to be recorded for every 11° of rotor azimuth position. The horizontal resolution of this system is limited to approximately 250 lines. Therefore, a close focus was needed to get a good angular measurement of the tufts. Various magnifications were used to maximize resolution and field of view. Information recorded on video tape was processed using video-image computer processing techniques.

3.3 Lighting

We tes at night to avoid the thermal drifting of the strain gages that would result from uneven blade heating in sunlight. This required lighting to illuminate the white tufts for the video camera. So, we placed 11 tungsten halogen 120-V spotlights along the camera boom and aimed at the blade; the lights were focused along the outboard 50% of the blade span. The video pixel intensity of a tuft was 35 on a gray scale of 0 to 256, while the black background was 10 to 15; the contrast was great enough so that the tufts could be seen easily. Unfortunately, there was still not enough light to operate the camera shutter, and moving images were blurred on the video display.

3.4 Angle-of-Attack Transducers

An accurate measurement of the blade AOA would be very useful in correlating wind tunnel data, analytical data, and test data. Unfortunately, this is also one of the most difficult measurements to make. Local flow is affected by the blade-induced velocity, which distorts measurements. The stagnation-point location has been used to indicate angle of attack but has been shown to produce erratic results. In atmospheric tests, a wind vane was used (3) that would align itself with the flow and indicate AOA. The vane was mounted on a probe attached to the nose of instrumented aircraft. This approach proved to be accurate (after analytical corrections), although reliability is a question. Sandia National Laboratories (SNL) attempted, with marginal success, pressure sensing of the AOA using a five-hole probe; however, unsteady effects appeared to cause problems.

We decided that the National Center for Atmospheric Research (NCAR) vane approach was best for the first attempt at measuring AOA. We developed a transducer based on the NCAR approach, but with some improvements. We used this transducer during testing to measure AOA on the turbine blade with some success. However, two problems surfaced:

1. The vane is influenced by the local induced velocity.
2. The vane is slightly underdamped, which causes it to ring at excitation frequencies above 10 Hz.

We corrected these problems by

1. Making wind tunnel measurements of the induced velocity corrections and applying them to the measured data
2. Using an inverse transfer function to correct for the dynamic characteristics of the vane.

These corrections have improved the accuracy of the AOA measurements.

3.5 Pressure Measurements

Measuring pressure distributions on the rotating blade presented some problems. The pressures are typically less than 0.07 N/m^2, a bandwidth of 0-100 Hz was needed, and many channels must be measured in a small area of the blade surface without disturbing the surface contour. As mentioned earlier, our approach was to mount a 32-tap ESP-32 pressure transducer inside the blade (Figure 5). We installed small stainless-steel tubes (less than 0.5 m in length) in the blade to carry surface pressures to the transducer. To document the dynamic effect of the tubes on measured pressures, we measured transfer functions between applied surface pressures and pressures measured by the transducer. Minimal distortion occurs below 50 Hz, but significant amplification occurs from 50 to 100 Hz. To compensate for this distortion, we used an inverse transfer function to correct the high-frequency pressure measurements. This technique is described in (4).

We chose the ESP-32 pressure transducer made by Pressure Systems International (PSI) because of its compact size and pressure sensitivity. Another advantage to the ESP-32 transducer is that it can be calibrated by remote control and can therefore be calibrated while the turbine is rotating. It is also convenient to calibrate frequently to document any zero drift, which is common in some solid-state pressure transducers. We developed a control system to control the ESP-32 calibrations and condition the output

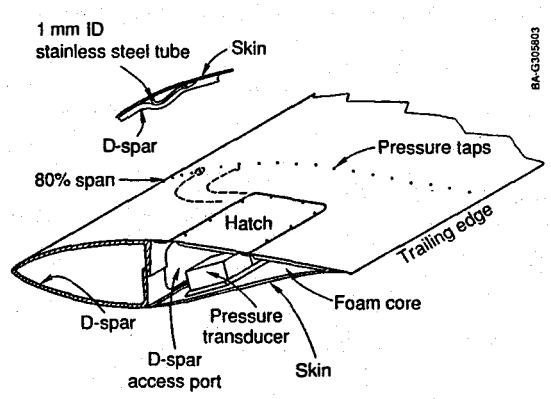

Fig. 5. Pressure transducer layout on the wind turbine blade

signal to achieve a sample rate of 522 Hz per pressure tap. This system is used to perform calibrations every 5 min of test operation. The frequent calibration resulted in data that are accurate to 2% (0.001 N/m^2) of the expected dynamic pressure.

The 32 pressure taps were located at 80% of full blade span, where the Reynolds number is approximately 10^6. The taps were aligned along the chord (instead of being staggered) so that spanwise variations in pressure distributions would not distort measured chordwise distributions. The chordwise spacing of the pressure taps is shown in Figure 6. In addition to the pressure taps indicated on Figure 6, there are two Kulite Model LQ-125-5 surface-mount pressure transducers (at locations 10 and 17 on the figure).

3.6 Anemometers

We used a variety of anemometers. The primary near-field data were provided by anemometers mounted on the vertical-plane array and the near-field met tower (Figure 4). Additionally, far-field atmospheric stability data were provided at the test site's 50-m north met tower.

The vertical-plane array of R. M. Young three-axis prop anemometers provided low-frequency (0-1 Hz) wind-shear data, azimuthally varying wind data, and low-frequency inflow statistics. High-frequency (0-10 Hz) data were provided by a three-axis sonic anemometer mounted at hub height on the near-field met tower and two dual-axis hot-wire anemometers mounted 1.2 m below hub height.

We recorded far-field atmospheric data at the north met tower. These data included temperature gradient (Richardson number), wind shear up to 50 m, and wind directions at four different altitudes.

3.7 Strain Gages

Strain gages measured blade, tower, rotor, and yaw loads. Table 1 shows the pulse code modulation (PCM) configurations and data rates on each PCM stream. Blade flapwise and edgewise loads were monitored at eight different spanwise locations. Pitching moment (i.e., blade torsion) was monitored at three spanwise locations. Figure 7 shows the locations of all the blade strain gages. We took the load measurements to establish reliable blade-load distributions to help us confirm measured aerodynamic (applied) loads.

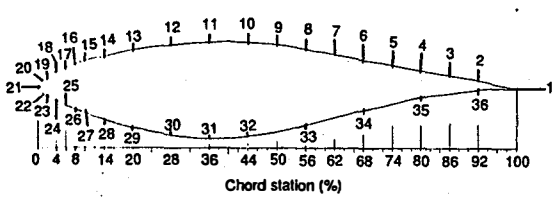

Fig. 6. Pressure tap locations on the blade

TABLE 1. PULSE CODE MODULATION CONFIGURATIONS

PCM	Bit Rate (Kbit/s)	Sample Rate (Hz)	Number of Channels	Delta T (ms)	Description
1	7.5	34.72	16	28.2	North Met
2	15.0	69.44	16	14.4	VPA
3	60.0	277.78	16	3.6	Local Met
4	400.0	520.83	62	1.92	Rotor
5	60.0	277.78	16	3.6	Turbine

Each strain gage bridge was made up of four active gage elements mounted inside the fiberglass blade skin. We placed the gages inside the skin to preserve the exterior airfoil shape and surface smoothness.

We were careful to position the strain gages to minimize flapwise and edgewise crosstalk. However, measurable crosstalk was apparent during the blade pull and strain-gage calibration tests. To eliminate this error, we measured the crosstalk calibration coefficients and used them to correct the measured data.

4. WIND TUNNEL TESTS

The S809 airfoil used in the Combined Experiment underwent two wind tunnel test programs. The first one was to confirm that the airfoil performed according to design specifications, because the airfoil was designed using a computer code. A very accurate and smooth test model was used with more than 100 pressure taps. The Delft Technical University wind tunnel in Holland was used because of its extremely low turbulence level. The test matrix included steady-state data runs at Reynolds numbers from 1 to 3 million. We also acquired data from rough and smooth conditions, along with oil-film flow-visualization tests. These test results can be considered the reference two-dimensional airfoil data set, and we will compare all future wind tunnel data and rotating, three-dimensional pressure data to this set.

A second wind tunnel test was conducted at Ohio State University (OSU) in an open-circuit wind tunnel measuring 0.92 m x 1.53 m (3 ft x 5 ft). This test was conducted to establish a credibility link between the Delft data, the test airfoil, and SERI

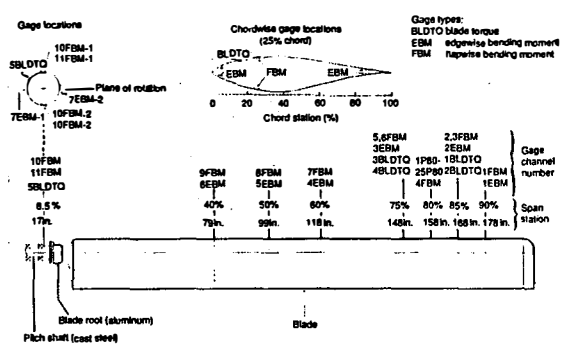

Fig. 7. Strain gage locations on the blade

instrumentation. At OSU, the wind tunnel test model was fabricated in the same molds that were used to make the test blade. Pressure taps were located in exactly the same positions as those on the test blade, and the same pressure transducer was used in the rotating blade test and the wind tunnel. We then compared the data measured from the OSU wind tunnel with the data from the Delft wind tunnel. We found some discrepancies as expected. After we documented the discrepancies, we established a credible basis for comparing three-dimensional pressure distributions with two-dimensional data.

5. PRELIMINARY RESULTS

5.1 Lift Coefficient

Figure 8 is a typical plot of lift coefficient versus AOA (labeled "Alpha") for Delft wind tunnel data and OSU data. The figure shows Delft data for the smooth condition. As shown, there is good agreement for AOA of less than 7°. When AOA is greater than 7°, the OSU lift coefficients are lower than the Delft coefficients by as much as 10% at $C_{l,max}$.

This difference could be caused by two factors. When pressure taps are lined up along the chord, as they were on the OSU model, the taps cause a roughness that in turn can cause premature transition of the boundary layer, adverse pressure gradients, and premature separation. The end result is that $C_{l,max}$ is lower. Another contributor could be the minimal number of pressure taps used in the OSU tests. The field tests will be limited to 32 pressure taps, so only 32 were used in the wind tunnel tests.

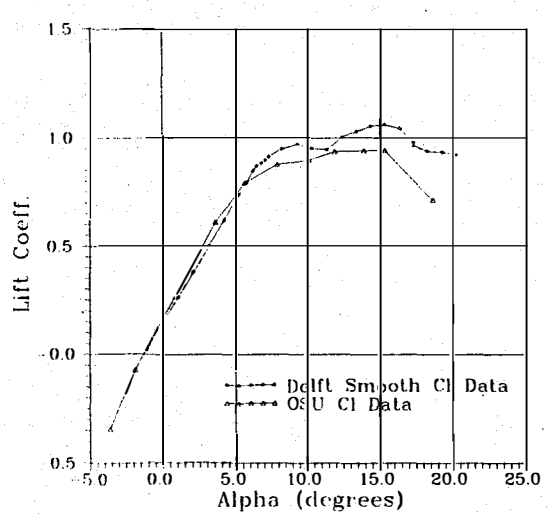

Fig. 8. Comparison of smooth lift curves for the Delft and OSU data

5.2 Flow Visualization

As mentioned earlier, we used "mini tufts" as our primary flow-visualization tool. Cooperative tests, involving SNL, were also conducted using liquid crystals (5) to investigate the boundary-layer mechanics. However, these results are mentioned only briefly in this report, and future reports will address the liquid-crystal results in more detail (6).

We made still shots by freezing a video frame with a Data Translation "Frame Grabber," which transferred the video image to a Compaq 386 computer, where we could enhance the image and print the enhanced image on a laser printer.

Because the images are poor reproductions, it helps to know that when a tuft is engulfed by laminar flow it remains steady and presents a clear image to the video camera. On the other hand, when a tuft is engulfed in separated flow, it dances around rapidly and presents a blurred image, barely visible on the video recording. Night testing compounded this problem because the darkness prevented using the camera's fast shutter. The shutter would normally freeze the image without blur, but it requires much more light than was available during the night. Viewing the videos themselves, it is far easier to see the angles of the tufts than it is when freezing the frame and displaying it on a hard copy.

By panning the video camera, we could record inboard flow patterns at a section in the 55%-65% span. The separation boundary at 65% span is still located at 55% chord, but inboard of the 60% span the boundary quickly sweeps toward the leading edge. Figure 9 shows the separation boundary location throughout the entire blade for this moderate-AOA operating condition.

Liquid crystals helped us to visualize the boundary-layer surface shear-stress patterns on the airfoil as part of a cooperative program with SNL. The purpose of these tests was to determine if the boundary-layer shear-stress patterns were modified by rotational effects. The S809 airfoil has a laminar separation bubble located at 58% chord at AOA = 0°, and it moves forward as AOA increases. A photograph of the blade shows a liquid-crystal color and rivulet pattern at AOA = 0°-5° that clearly identifies the location of this bubble at 55%-60% chord and confirms Delft wind tunnel measurements.

6. FUTURE WORK

Testing is not complete. We still need high-wind-speed, high-AOA data to study modifications to stall behavior on the rotating blade. We will conduct detailed analyses of

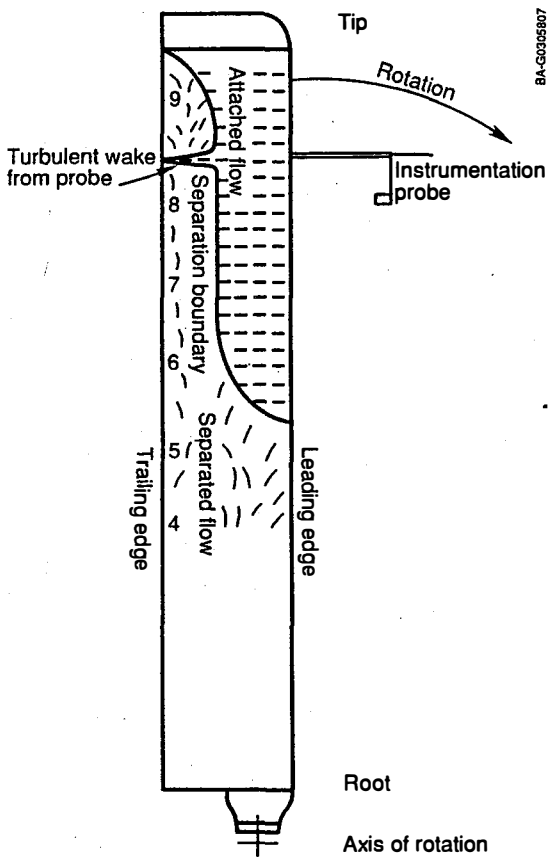

Fig. 9. Location of the separation boundary on the blade

pressure distributions and integrated aerodynamic force coefficients. A very important area yet to be investigated is how these measured aerodynamic loads correlate with dynamic blade loads. This kind of investigation will help designers predict damaging fatigue loads more accurately. We will perform studies on how to reduce or avoid such loads.

We also plan to study pitch control versus stall control of wind turbine power to see if dynamic loads can be relieved through aerodynamic stall regulation. We will study yawed operation to investigate the source of high dynamic loads and yaw stability.

Regarding inflow, we will use vertical-plane array data and atmospheric boundary layer data to investigate which atmospheric conditions are most damaging and which are most productive. This work will help wind prospectors differentiate between potentially damaging sites and productive sites.

7. CONCLUSIONS

More testing in higher wind speeds is needed before major conclusions can be drawn about the three-dimensional affects on the stall behavior of a rotating wind turbine blade.

At low AOA, this S809 airfoil appears to behave much like it would in two-dimensional, wind-tunnel-type flow.

It appears that the aerodynamic environment, in which the wind turbine blade operates, is unsteady.

8. ACKNOWLEDGMENTS

Many people at SERI and outside of SERI have contributed to this work. Not all can be mentioned here, but credit should be given to Walt Musial, Dave Simms, George Scott, and Mike Jenks for their major contributions. Dan Reda of SNL provided the liquid-crystal expertise in the boundary-layer tests. Bob Akins of Washington and Lee University, and Craig Hansen of the University of Utah, also provided valuable advice and guidance. Also, Al Eggers has been very helpful in his theoretical contributions to the test program. Finally, Bob Thresher provided inspiration and much appreciated technical support.

9. REFERENCES

(1) Tangler, J. L. and Somers, D. M., "Status of the Special-Purpose Airfoil Families," Proceedings of Windpower '87, SERI/CP-217-3315, American Wind Energy Association, Arlington, Virginia, 1988.

(2) Rae, W. H. Jr. and Pope, A., Low-Speed Wind Tunnel Testing Second Edition, John Wiley & Sons, New York, 1984, p. 133.

(3) Lenschow, D. H., "Vanes for Sensing Incidence Angles of the Air from an Aircraft," Journal of Applied Meterology, Vol. 10, No. 6, 1971, pp. 1339-1343.

(4) Irwin, H. P. H. H., Cooper, K. R., and Girard, R., "Correction of Distortion Effects Caused by Tubing Systems in Measurements of Fluctuating Pressures," Journal of Industrial Aerodynamics, Vol. 5, 1979, pp. 93-107.

(5) Reda, D. C., "Liquid Crystals for Unsteady Surface Shear Stress Visualization," AIAA 88-3841CP, First National Fluid Dynamics Congress, Cincinnati, Ohio, July 25-28, 1988.

(6) Reda, D. C. and Butterfield, C. P., "Liquid-Crystal/Shear Stress Visualization on a HAWT," Proceedings of Eighth ASME Wind Energy Symposium, January 1989.